Materials Research Express

PAPER

# Effect of $TiO_2$ content on the microstructure and mechanical and wear properties of yttria-stabilized zirconia ceramics prepared by pressureless sintering

Materials Research Express

PAPER

# Effect of $TiO_2$ content on the microstructure and mechanical and wear properties of yttria-stabilized zirconia ceramics prepared by pressureless sintering

RECEIVED
16 September 2019

REVISED
3 January 2020

ACCEPTED FOR PUBLICATION
14 January 2020

PUBLISHED
24 January 2020

**Pan Luo**[1], **Jin Zhang**[1], **Zongying You**[1], **Xuelin Ran**[1], **Yuhong Liu**[2], **Songxia Li**[1] **and Shuai Li**[1]

[1] School of Materials Science and Engineering, Southwest Petroleum University, Chengdu 610500, People's Republic of China
[2] Sichuan Yinhe Chemical Co., Ltd, Mianyang 622656, People's Republic of China

**E-mail:** jzhang@swpu.edu.cn

**Keywords:** titania, zirconia composite ceramics, mechanical properties, wear resistance

## Abstract

A yttria-stabilized zirconia ceramic is prepared by pressureless sintering at 1350 °C, and the effects of $TiO_2$ additive (0–10.0 wt%) on the microstructure, phase composition, and mechanical properties of the ceramic are investigated. The ceramic with no added $TiO_2$ consists mainly of a monoclinic phase with a few tetragonal phases. With increasing $TiO_2$ content, more t-$ZrO_2$ phases are stabilized to room temperature, and a new phase, $ZrTiO_4$, forms when the content of the $TiO_2$ excess reaches 5 wt%. $TiO_2$ facilitates the elimination of pores in the YSZ ceramics and increases the densification of the YSZ ceramics. The relative density increases from 91.5% ($TiO_2$ 0 wt%) to 96.2% ($TiO_2$ 10 wt%). Performance test results show a maximum bending strength of 312.56 MPa when the $TiO_2$ content of reaches 10 wt%. The micro-hardness and wear resistance of the YSZ ceramics first increases then decreases as the $TiO_2$ content increases, and the maximum micro-hardness and best wear resistance occur when the $TiO_2$ is added at 5 wt%; the maximum micro-hardness and the minimum volume wear rate is 1792.5 HV and 2.06 $\times$ $10^{-4}$ $mm^3$ $N^{-1}$ $\times$ m, respectively. The wear mechanism of the ceramic is mainly plastic deformation and microcracking, and the fracture mechanism is mainly intergranular fracture. These results show that $TiO_2$ is an effective sintering additive that promotes more t-$ZrO_2$ phases stabilized at room temperature, with acceptable mechanical and wear resistance properties.

## 1. Introduction

In recent years, oxide ceramic materials have been widely used because of their excellent mechanical properties. Ceramics on the base of refractory oxides, in particular on the base of zirconia ($ZrO_2$), are in the greatest demand because of their good physical and chemical properties (hardness, strength, chemical resistance, and crack resistance, etc) [1]. $ZrO_2$ has a high melting point of 2,700 °C and low electrical and thermal conductivity; therefore, it is commonly used as engineering material [2]. Moreover, $ZrO_2$ ceramics are also used as practical biological materials because of their good biocompatibility [3]. On the other hand, $ZrO_2$ is often used as a second phase to toughen other oxide ceramics, such as Zirconia Toughened Alumina (ZTA) [4]. $ZrO_2$ has three phases: (1) when the temperature is higher than 1380 °C, cubic $ZrO_2$ is stable; (2) when the temperature is lower, the $ZrO_2$ will be in the tetragonal phase; and (3) as the temperature decreases below 1200 °C, the tetragonal phase will become the monoclinic phase [2]. During thermal cycling of $ZrO_2$ ceramics, the phase transition from tetragonal to monoclinic has an 8% volume expansion that causes serious overall cracking of the material. Therefore, many applications of $ZrO_2$ ceramics require alloying with alkaline earth oxides or rare earth oxides in order to give $ZrO_2$ ceramics a completely or partially stable structure. For example, in 1975, partially stabilized $ZrO_2$ (PSZ) ceramics were prepared by Garvie in Australia with CaO as the stabilizer. For the first time, the toughening effect of the martensitic transformation of $ZrO_2$ was used to improve the toughness and strength of ceramics, greatly expanding the application of $ZrO_2$ in the field of structural ceramics [5].

**Table 1.** Particle size and purity of raw material powders.

| Raw material | Particle size | Purity |
|---|---|---|
| $ZrO_2$ | $\leqslant$3.5 $\mu$m | $\geqslant$99.0% |
| $TiO_2$ | $\leqslant$0.6 $\mu$m | $\geqslant$99.0% |
| $Y_2O_3$ | $\leqslant$7.5 $\mu$m | $\geqslant$99.99% |

Yttria ($Y_2O_3$) containing $Y^{3+}$ cations is used most frequently for $ZrO_2$ stabilization. Such a system is called yttria-stabilized zirconia (YSZ). An addition of 3 to 8 mol% of yttria is sufficient to stabilize the tetragonal $ZrO_2$ phase to room temperature (a partially stabilized YSZ). When yttria content exceeds 8 mol%, the high-temperature cubic $ZrO_2$ phase is stabilized by the cation solid solution (a fully stabilized YSZ) [6]. A YSZ ceramic has many excellent properties, for example, high ionic conductivity, thermal stability, and excellent mechanical properties. It is usually be used in high temperature electronic equipment due to a good special working environments adaptability, such as oxygen sensors, solid oxide fuel cells, and thermal barrier coatings [7–10].

The preparation of ceramic materials often requires a high sintering temperature. The sintering temperature of tetragonal polycrystalline $ZrO_2$ (TZP) ceramics is usually around 1600 °C, with high energy consumption, strict requirements on sintering equipment, and high cost, all of which lead to the limitation of ceramic material in application. Therefore, it is important to reduce the sintering temperature and improve the sintering performance of ceramics with an additive.

Some stabilizers have been reported as promoting the sintering and improving the performance of ceramics, such as $Si_3N_4$, MgO, CaO, $Al_2O_3$, and $TiO_2$ [4, 11–14]. Even blast furnace slag has been reported to reduce the sintering temperature and improve the strength of the ceramics [15]. Among them, $TiO_2$ is popular because of its environmental friendliness and low price. Addition of $TiO_2$ has been reported to promote the sintering and grain growth of $\alpha$- or transition-alumina [16–20]. The benefits are believed to be the result of the enhanced diffusivity due to the increasing concentration of the $Al^{3+}$ vacancies, as generated by $Ti^{4+}$ substituting for $Al^{3+}$ [16]. $TiO_2$ improves the sintering performance of $ZrO_2$ ceramics in a similar manner [21, 22].

Some studies have investigated the $TiO_2$-YSZ ceramic system. Tsukuma *et al* examined the effect of $TiO_2$ on the optical properties of a YSZ ceramic [23]. Miyazaki *et al* evaluated the structural, thermal, and electrical properties of $TiO_2$-3YSZ and $TiO_2$-8YSZ ceramics [13, 24]. Chen *et al* investigated the phase stability, microstructural evolution, and room temperature mechanical properties of cubic $ZrO_2$ doped with $TiO_2$ and stabilized with 8 mol% $Y_2O_3$ [25].

Although the electrical, optical, and thermal properties of $TiO_2$-YSZ ceramics have been evaluated in past studies, the available literature suggests that the effects of $TiO_2$ content on the densification and wear behavior of YSZ ceramics have not been investigated. Moreover, the sintering temperature of $ZrO_2$ above 1600 °C easily causes a large grain size. To solve the contradiction between densification and having a fine grain size in atmospheric sintering, low temperature sintering is needed. A temperature of 1350 °C has been selected for this study, and the YSZ ceramic samples with various $TiO_2$ content has been prepared via pressureless sintering. The influence of the amount of $TiO_2$ on the relative density, microstructure, and mechanical and wear resistance properties of the YSZ ceramic have been fully investigated. The phase evolution in the ceramic substrate during sintering has also been analyzed.

## 2. Experimental procedures

### 2.1. Ball milling and mixing of powders

Zirconium dioxide and titanium dioxide (both from the Kelon Chemical Reagent Factory, Chengdu, China) were used as the raw materials. Kelon's $Y_2O_3$ was the stabilizer. The particle size of the raw materials is given in table 1. The three powders were mixed in a PMQ2L planetary ball mill (DPLIFT Machinery Equipment Company Limited, ShangHai, China) with a corundum mill and balls. Our previous experiments had shown that the optimum sintering process could be obtained when the content of $Y_2O_3$ is 5.5 wt%. The amount of $TiO_2$ added was between 0 and 10.0 wt%, and the rest of the mixture was $ZrO_2$. ($TiO_2$ has a lower hardness and elastic modulus compared with $ZrO_2$. Therefore, considering the mechanical properties of the samples, the amount of $TiO_2$ was kept below 10 wt%.) The ball milling time was 12 h, and the rotation speed was 400 r $min^{-1}$. Absolute ethanol was the ball milling medium. The particle size of the raw materials after ball milling is around 0.5 $\mu$m and 2.5 $\mu$m, as shown in figure 1.

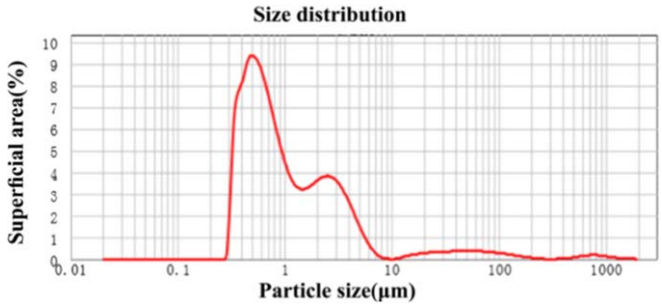


**Figure 1.** The particle size distribution of the raw materials after ball milling.

### 2.2. Granulation of powder

The slurry obtained by ball milling was placed in a 101A-2ET electrothermal blast air oven (ShangHai Laboratory instrument Works Co., Ltd, ShangHai, China) at a temperature of 80 °C until the absolute ethanol in the slurry volatilized. The dried powder was then milled in a mortar and sieved through a 0.15 mm sieve. Polyvinyl alcohol (PVA, 5 wt%, Kelon Chemical Reagent Factory, Chengdu, China) was added to the powder as a binder after the first sieving, and then the mixture was sieved again. Finally, particles with a size between 0.15 mm and 0.8 mm were selected as the molding material.

### 2.3. Pressure molding of bulk

To improve the compactness of the green body, two-step compression molding was carried out. First, the SB hand-operated sample making machine (Xiangtan Xiangyi Instrument Co., Ltd, XiangTan, China) was used. After granulation, a two-way force was applied to combine the particles after granulation into a preliminary geometric shape. As the samples were subjected only to axial pressure, the shrinkage performance in other directions could not be guaranteed. To make the whole bulk more uniform and compact, the bulk obtained from the first pressing was put into a DJY60/120–200 cold isostatic press (Taiyuan Magnetic Source Co., Ltd, TaiYuan, China). This second pressing subjected the bulk to pressure from all directions, reducing its porosity and improving the subsequent sintering density.

### 2.4. Sintering

The samples obtained from the press molding were placed in a STGS-80-14 tube furnace (SANTC Furnace Technology Co., Ltd, HeNan, China) for rubber discharging and pre-sintering. The heating rate was 10 °C $min^{-1}$. When the temperature reached 600 °C, it was held for 1 h to remove PVA from the samples. Then, it was heated to 1000 °C and held for 2 h. The samples were then cooled to room temperature inside the furnace.

The purpose of pre-sintering is to remove any stress remaining in the samples after the press molding and to avoid having any residual stress that could affect the samples during the final sintering.

The samples obtained by pre-sintering were placed in the tube furnace for final sintering with a temperature of 1350 °C, a heating rate of 10 °C $min^{-1}$, and a holding time of 2 h. Then, the temperature was dropped to 800 °C at a rate of 5 °C $min^{-1}$, and the samples were then cooled to room temperature inside the furnace.

### 2.5. Characterization

The radial and axial dimensions of the bulk ceramic (figure 2) before and after sintering were measured using a vernier caliper to calculate shrinkage.

The shrinkage calculation is shown in Formulas (1.1) and (1.2):

$$S1 = (d0 - d)/d0 \times 100\% \quad (1.1)$$

$$S2 = (h0 - h)/h0 \times 100\% \quad (1.2)$$

where $S_1$ is the radial shrinkage, $S_2$ is the axial shrinkage, $d_0$ is the diameter of the sample before sintering, $d$ is the diameter of the sample after sintering, $h_0$ is the height of the sample before sintering, and $h$ is the height of the sample after sintering.

The bulk densities of the sintered samples were calculated using Archimedes' method performed with an ET-120HM electronic densitometer (Etnaln Electronics Technology, Co., Ltd, BeiJing, China). The relative density of each sample was calculated according to Formula (1.3):

$$K = \rho/\rho 0 \quad (1.3)$$

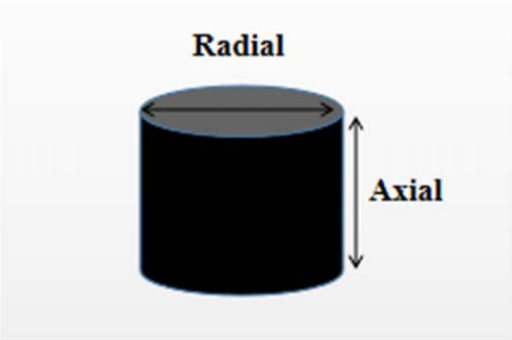


**Figure 2.** Schematic diagram of sample dimensions.

where $K$ is the relative density, $\rho$ is the experimentally measured sample density and $\rho_0$ is the theoretical density of the sample. The phase composition of the ceramics was measured by x-ray diffraction (XRD; DX-2700B, Haoyuan Instrument Co., Ltd, DanDong, China).

The bending strength of the samples was tested using an electromechanical universal testing machine (MTS Systems Co., Ltd, DanDong, ShangHai, China). The loading rate was 0.5 mm $min^{-1}$, and the sample size being tested was 30 × 5 × 3 mm.

The microstructure of the samples was observed using scanning electron microscopy (SEM; MA15, Carl Zeiss AG, Germany). The surface and cross section of the samples were observed to determine the crystal growth and fracture mode of the substrate.

An HV-1000A Vickers microhardness tester (Laizhou Huayin Testing Instrument Co., Ltd, Laizhou, China) was used to determine the hardness. The loading condition was 1000 gf/15 s, and the surface-projected diagonals of the indented area were measured by optical microscopy to calculate hardness.

An MFT-4000 multi-functional tester for material surface (State Key Laboratory of Solid Lubrication, Lanzhou, China) was used to determine the friction coefficients of the samples. Because of their high hardness, super corrosion resistance, and high fatigue resistance, AISI 52100 (GCr15) steel balls are widely used in petroleum and other engineering fields [26]. Since the ceramic materials prepared in this study are also used in the petroleum field, a reciprocating friction method was applied using a GCr15 grinding ball with a load of 30 N; the rubbing speed was 50 mm $min^{-1}$; the wear scar length was 10 mm, and the test time was 60 min.

## 3. Results and discussion

### 3.1. Relative density of the $TiO_2$-YSZ ceramics

Figure 3 illustrates the relative densities of YSZ ceramics with different $TiO_2$ contents. (All error bars in this paper represent standard deviation.) The samples with no added $TiO_2$ have low relative densities, which improves with an increase in the $TiO_2$ content. When the content of $TiO_2$ reaches 10 wt%, the samples have the largest relative density of 96.2%. These results indicate that adding $TiO_2$ improves the sintering densification of YSZ ceramics. The beneficial mechanism may be that $T^{4+}$ can replace $Zr^{4+}$ in $ZrO_2$ to form a substitutional solid solution, and increasing the $TiO_2$ content in the YSZ ceramic promotes the formation of defects; the $T^{4+}$ dissolves in the $ZrO_2$ enhanced diffusivity and the sintering process, thereby obtaining a higher relative density. The phenomenon of enhanced sinterability is similar to that seen in past research on alumina/zirconia ceramics with added $TiO_2$ [27]. The increase in relative density indicates a decrease in the porosity of the ceramic substrate, which corresponds to better mechanical properties.

Table 2 lists the shrinkage of samples with different amounts of $TiO_2$ content after sintering. Both radial and axial shrinkage increases with an increase in $TiO_2$ content. This result also confirms that adding $TiO_2$ promotes the sintering process and improves the relative density of YSZ ceramics.

### 3.2. XRD patterns of $TiO_2$-YSZ ceramics

Figure 4 illustrates the XRD patterns of the samples with varying $TiO_2$ contents. When the content of $TiO_2$ is low, only $ZrO_2$ is detected, and the main phase is m-$ZrO_2$ because the other added components are dissolved into the $ZrO_2$. With an increase in $TiO_2$ content, the peak of the m-$ZrO_2$ phase decreases, and the peak of the t-$ZrO_2$ phase increases; the major phase in the YSZ ceramic substrate becomes t-$ZrO_2$, and the new phases $TiZrO_4$ and c-$ZrO_2$ are detected.

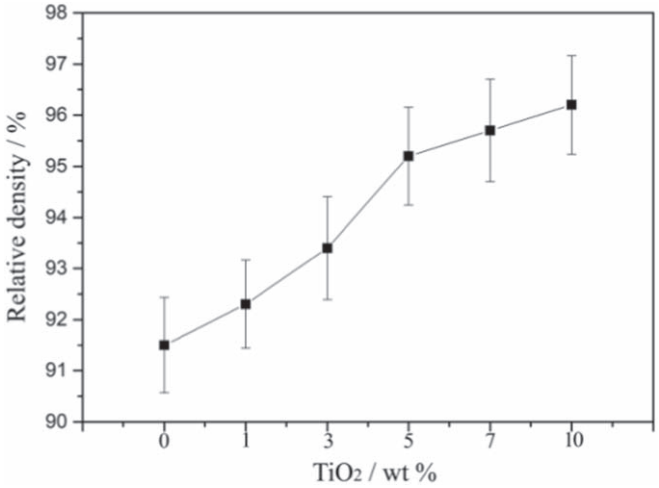


**Figure 3.** The relative densities of samples with different $TiO_2$ contents.

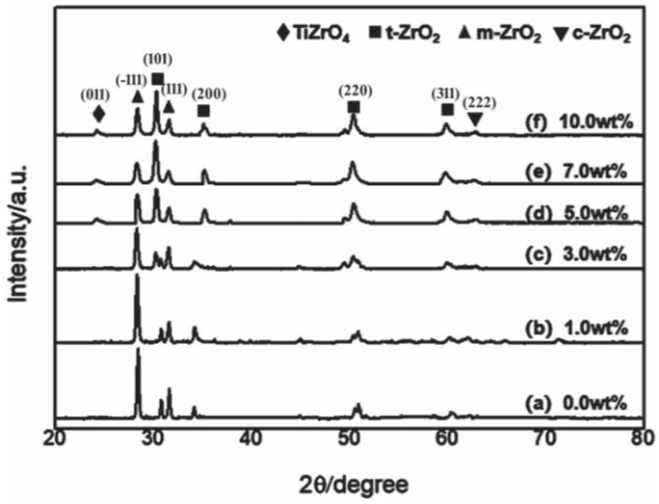


**Figure 4.** XRD patterns of $ZrO_2$ samples sintered at 1350 °C for 2 h with various amounts of $TiO_2$ added: (a) 0 wt%, (b) 1.0 wt%, (c) 3.0 wt%, (d) 5.0 wt%, (e) 7.0 wt%, and (f) 10.0 wt%.

**Table 2.** The shrinkage of samples with different $TiO_2$ contents.

| | Shrinkage (%) | |
|---|---|---|
| $TiO_2$ content (wt%) | Radial | Axial |
| 0 | 17.65 | 18.01 |
| 1 | 18.05 | 18.72 |
| 3 | 18.54 | 19.31 |
| 5 | 19.42 | 20.07 |
| 7 | 20.01 | 20.54 |
| 10 | 21.53 | 23.27 |

Figure 5 is a binary phase diagram of $TiO_2$ and $ZrO_2$. It shows that the main phase region of $TiZrO_4$ is at 1700 °C. However, previous research by McHale *et al* [28] showed that the $TiZrO_4$ phase can be stable above 1100 °C. This result suggests that the addition of $TiO_2$ contributes to the stability of the tetragonal phase at room temperature. The reason is that Ti ions can dissolve in $ZrO_2$ and act as a stabilizer. These dissolved ions also expand the average radius of the cations, enabling the tetragonal phase to obtain a more stable structure with a

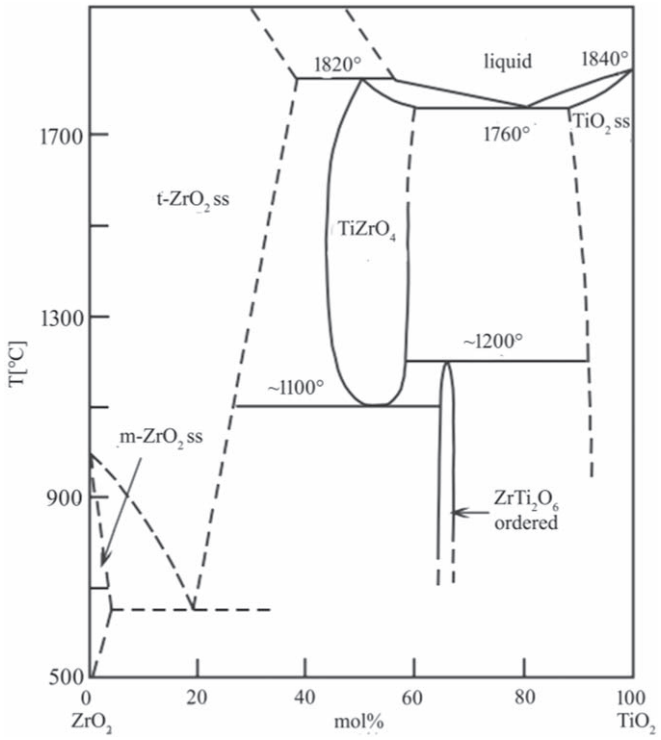


**Figure. 5.** The $TiO_2$–$ZrO_2$ binary phase diagram [29].

coordination number of eight and stabilizing the phase at room temperature. The t-$ZrO_2$ phase has a higher density compared with m-$ZrO_2$. Thus, the transition of m-$ZrO_2$ to t-$ZrO_2$ is accompanied by a volumetric shrinkage of 3.0 to 4.0%, which is one of the reasons why adding $TiO_2$ can increase the density of $ZrO_2$.

### 3.3. SEM micrographs of $TiO_2$-YSZ ceramics

Figure 6 illustrates the surface morphology of the samples with the different contents of $TiO_2$. The microstructure of samples with $TiO_2$ content of 0 wt% and 1 wt% showed that the substrate had poor compactness, and the visible pores were observed at a lower magnification (figures 6(a) and (b)). Moreover, the grain profile indistinct under the scanning electron microscope, and it is difficult to observe the intergranular grains of $ZrO_2$ due to the presence of the liquid phase [3, 30]. In contrast, when the content of $TiO_2$ exceeds 3 wt%, the densification of YSZ ceramics is significantly improved due to the reduction of porosity, displaying a more continuous and compact microstructure (figures 6(c)–(f)). This is indicated that the addition of $TiO_2$ is conducive to sintering densification and eliminating porosity for YSZ ceramics, which is consistent with previous researches [21, 27]. In addition, as the content of $TiO_2$ increases from 3 wt% to 10 wt%, a significant increase of grains size can be observed with the scanning electron microscope at a higher magnification. This is because the addition of $TiO_2$ promotes the grain growth of YSZ ceramics [31–33], the mechanism may be that the addition of $TiO_2$ enhanced the grain boundary migration, another possibility is the enhancement of the $ZrO_2$ diffusion coefficients by $TiO_2$ additive [30].

### 3.4. The micro-hardness of $TiO_2$-YSZ ceramics

Figure 7 shows the surface Vickers hardness of the $TiO_2$-YSZ ceramics as a function of $TiO_2$ content. The figure shows that when the content of $TiO_2$ is less than 5.0 wt%, the micro-hardness of the YSZ ceramic increases with an increase in the content of $TiO_2$, and a maximum value of 1792.5 HV is reached when the $TiO_2$ content is 5.0 wt%. This is because the $TiO_2$ facilitates the elimination of pores and increases the densification of the YSZ ceramics. The Vickers hardness is directly related to the bulk density [21]; the improvement in the relative density means that the hardness of the YSZ ceramics also increases.

However, the hardness presents a decreasing trend with any further increase of $TiO_2$. As the $TiO_2$ content increases from 5.0 wt% to 10.0 wt%, the hardness decreases from 1792.5 HV to 1508.1 HV. Although $TiO_2$ promotes the sintering densification of the YSZ ceramic, with its increase, $TiO_2$ and $ZrO_2$ form a new phase, $TiZrO_4$, as shown in figure 4. $TiZrO_4$ has a lower elastic modulus compared with $ZrO_2$ [34], which corresponds to a lower hardness [27]. In addition, previous literature has reported that the microhardness measures of $ZrO_2$, $TiO_2$, and $TiZrO_4$ to be around 15.75 GPa, 10.29 GPa, and 8 GPa, respectively [3, 35]. The hardness of the

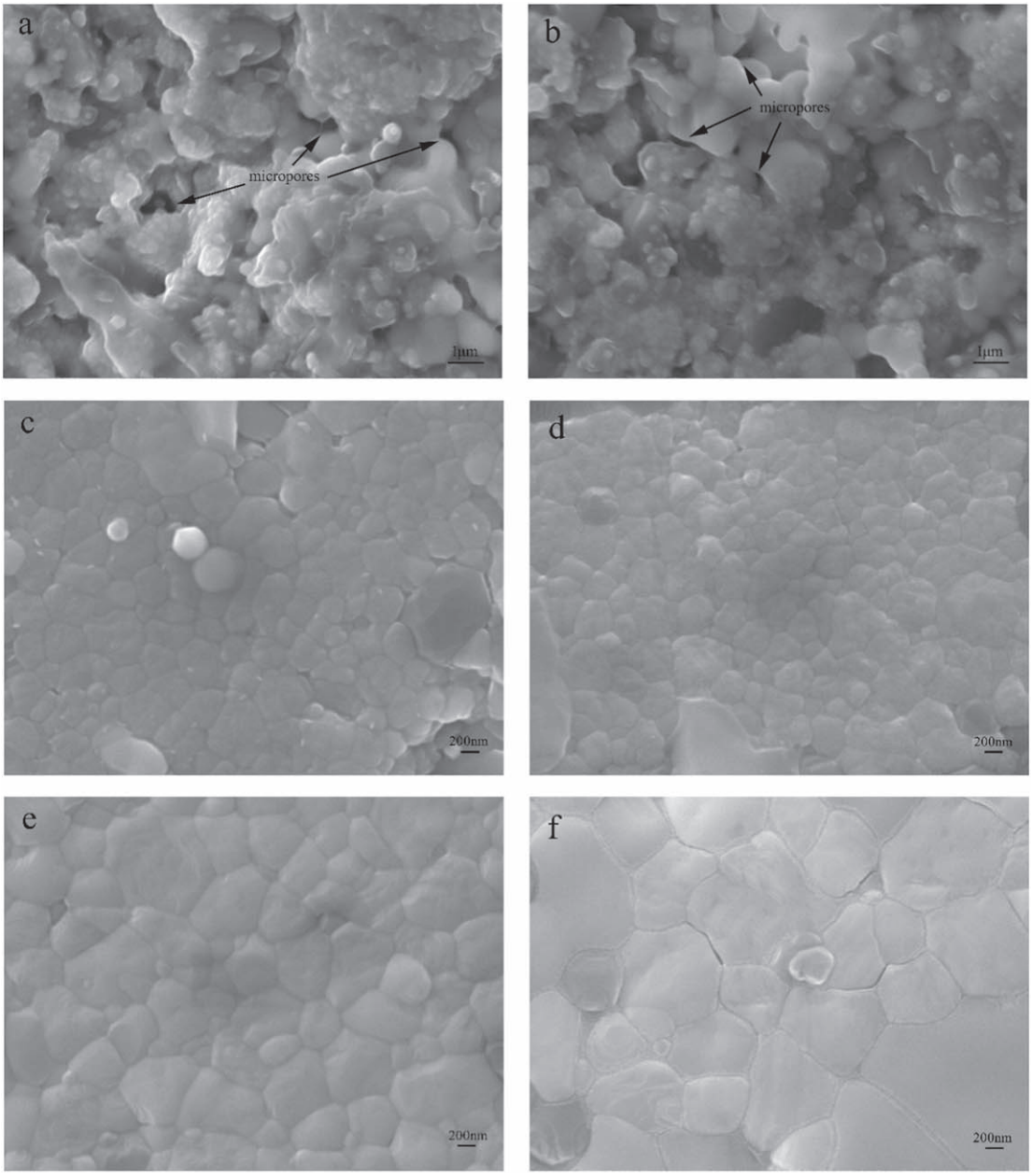


**Figure 6.** Surface micrographs of YSZ ceramics sintered at 1350 °C for 2 h with various amounts of $TiO_2$ added: (a) 0 wt%, (b) 1.0 wt%, (c) 3.0 wt%, (d) 5.0 wt%, (e) 7.0 wt%, and (f) 10.0 wt%.

composites possibly followed the mixture law [34]:

$$H_c = H_a V_{fa} + H_b V_{fb} \quad (2.1)$$

where $H_c$, $H_a$, and $H_b$ are the hardness of the composite, the component *a*, and the component *b*, respectively, whereas $V_{fa}$ and $V_{fb}$ are the volume fractions of the component *a* and the component *b*, respectively. With the increase of $TiO_2$ content, the volume fraction of $ZrO_2$ in the substrate is bound to decrease, resulting in a decrease of the hardness of the $TiO_2$-YSZ composites. On the other hand, as the $TiO_2$ content increases from 5.0 wt% to 10.0 wt%, the increase in grain size (figure 6) also affect the variation tendency in hardness.

### 3.5. The bending strength of $TiO_2$-YSZ ceramics

Figure 8 depicts the bending strength of the samples, obtained by a three-point bending test. The bending strength of the $TiO_2$-YSZ ceramic increases with an increase in $TiO_2$ content. The samples without added $TiO_2$ have the lowest bending strength at 196.13 MPa, and as the $TiO_2$ content increases to 10.0 wt%, the bending strength increases to 312.56 MPa. The bending strength of a ceramic is inversely proportional to its porosity, and the porosity is inversely proportional to density; therefore, the bending strength is related to the density. Thus, the addition of $TiO_2$ promotes the sintering densification of the YSZ ceramic and improves the bending

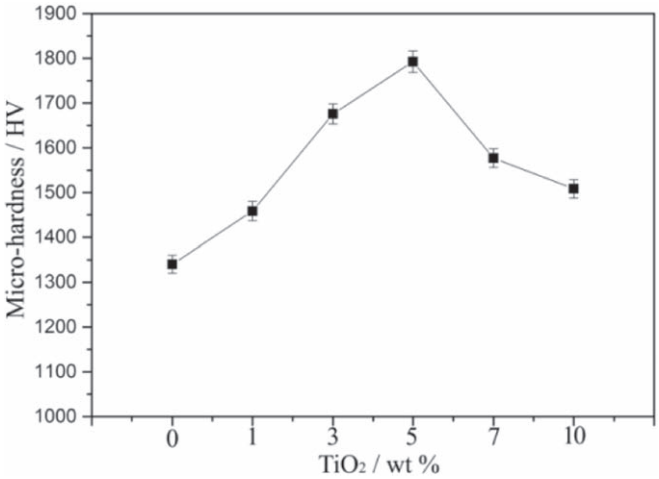


**Figure 7.** The micro-hardness of samples with different amounts of $TiO_2$ contents after sintering.

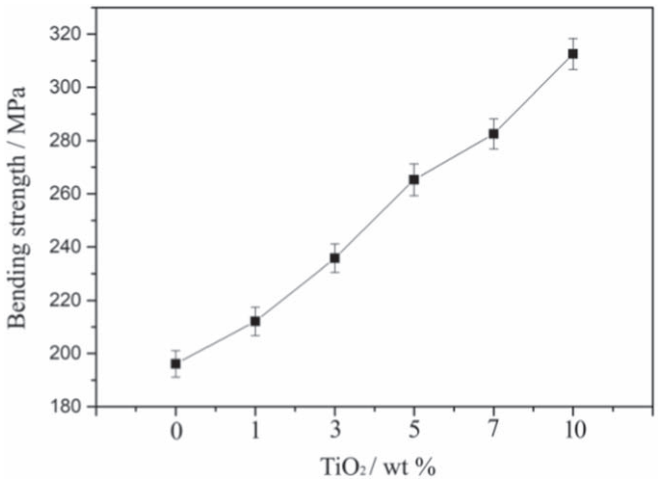


**Figure 8.** The bending strength of samples with different $TiO_2$ content.

strength. Another possibility is that the addition of the $TiO_2$ plays a role in second-phase pinning and in hindering crack propagation, thereby improving the bending strength [30].

Figure 9 shows the cross-section micromorphology of the YSZ ceramics with different amounts of $TiO_2$ contents. It is noted that, the cross-section micromorphology of the samples with 0 wt% and 1 wt% $TiO_2$ added (figures 9(a) and (b)) shows a high porosity, and it is difficult to observe the intergranular grains, which are consistent with the results observed in figure 6. In addition, there are some large grains observed, and the main components are determined to be Zr and O by EDS analysis (shown in figure 10, and the test area is marked by the rectangle in figure 9(b)). Therefore, it can be judged to be abnormally grown $ZrO_2$. It is possible that insufficient ball milling may have caused some large $ZrO_2$ particles to remain and grow further at high temperature. When the content of $TiO_2$ excess 3 wt% (figures 9(c)–(f)), the YSZ ceramics display a cross-section micromorphology with many holes due to the grains being pulled-out and some of grains break at some locations, which indicates that the fracture mechanism is mainly intergranular fracture [3, 27].

### 3.6. The wear resistance of $TiO_2$-YSZ ceramics

Figure 11 illustrates the relation between the coefficient of friction and time of the samples with different amounts of $TiO_2$ contents, and the average friction coefficient and wear scar area are shown in table 3. As the content of $TiO_2$ increases from 0 wt% to 5.0 wt%, the friction coefficient of the samples decreases, with the average friction coefficient decreases from 0.438 to 0.296. However, when the $TiO_2$ content exceeds 5.0 wt%, the friction coefficient increases somewhat, and when $TiO_2$ content reaches 10.0 wt%, the average friction coefficient increases to 0.342. A large number of studies have reported that the friction coefficient of a material is

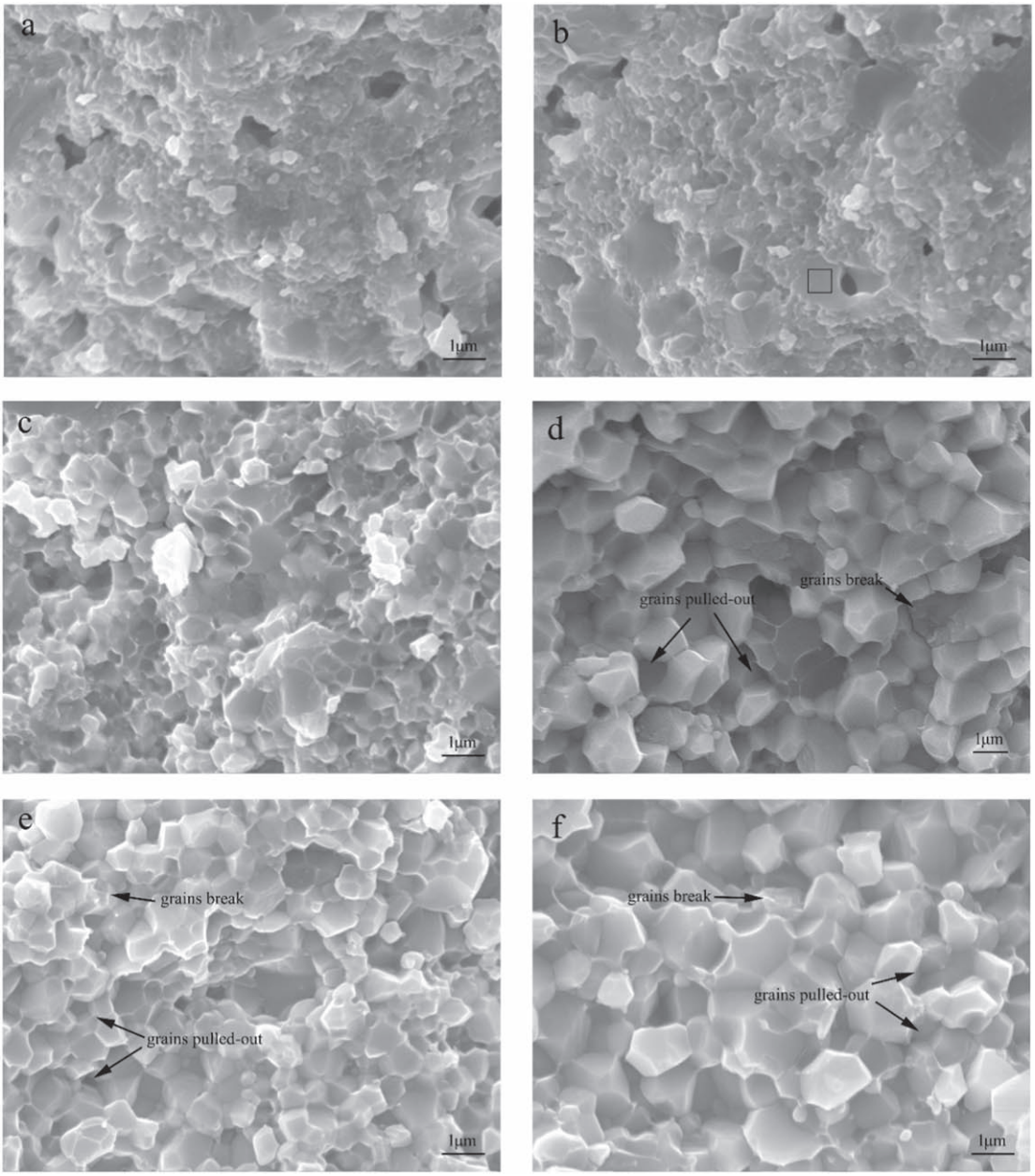


**Figure 9.** The cross-section micromorphology of YSZ ceramics sintered at 1350 °C for 2 h with different amounts of $TiO_2$ added: (a) 0, (b) 1.0 wt%, (c) 3.0 wt%, (d) 5.0 wt%, (e) 7.0 wt%, and (f) 10.0 wt%.

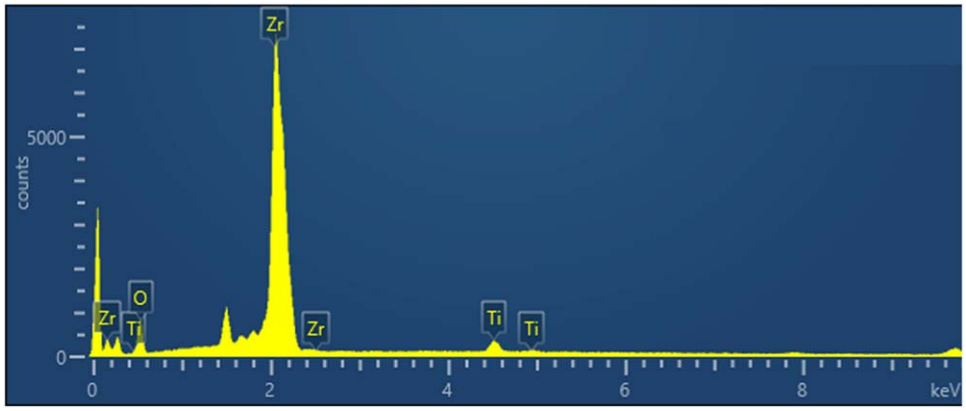


**Figure 10.** The energy spectra of YSZ ceramic cross-section grains.

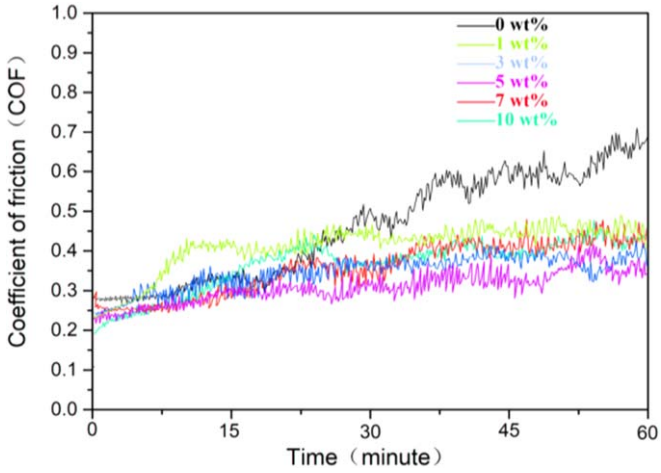


**Figure 11.** The relation between the coefficient of friction and wear time of the samples with different amounts of $TiO_2$ contents.

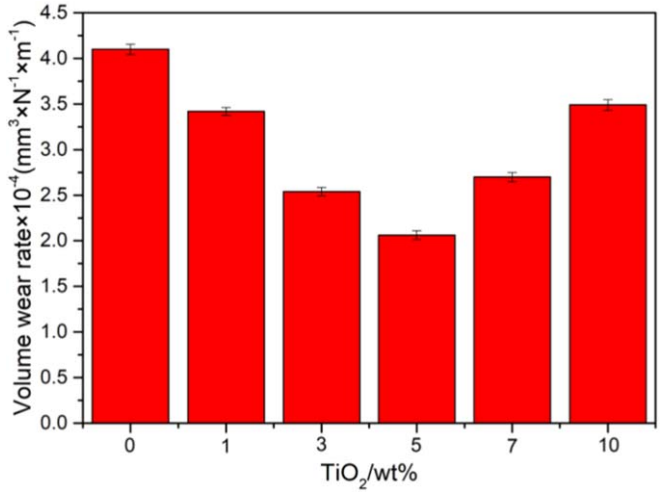


**Figure 12.** The volume wear rate of the YSZ ceramics as a function of $TiO_2$ content.

**Table 3.** The coefficient of friction and the wear scar area of the YSZ ceramics with different amounts of $TiO_2$ contents.

| $TiO_2$ (wt%) | Average friction coefficient | Wear scar area |
|---|---|---|
| 0 | 0.438 | 2.29 $mm^2$ |
| 1 | 0.384 | 3.14 $mm^2$ |
| 3 | 0.305 | 4.00 $mm^2$ |
| 5 | 0.296 | 5.24 $mm^2$ |
| 7 | 0.334 | 5.71 $mm^2$ |
| 10 | 0.342 | 6.13 $mm^2$ |

related to its grain size and mechanical properties [36–39]. When the content of $TiO_2$ increases from 0 wt% to 5.0 wt%, the densification and the hardness of YSZ ceramics is increases, resulting in a decrease in the friction coefficient of the YSZ ceramics. With a further increase of $TiO_2$ content, the grains size increases and the hardness decreases, moreover, the mass percentage of $TiO_2$ and $TiZrO_4$ increases which have a smaller elasticity modulus compared with $ZrO_2$ [27, 40, 41], so that the friction coefficient tends to increase.

Figure 12 depicts the relationship between the volume wear rate of the YSZ ceramics and the $TiO_2$ content, calculated by Formula (2.2):

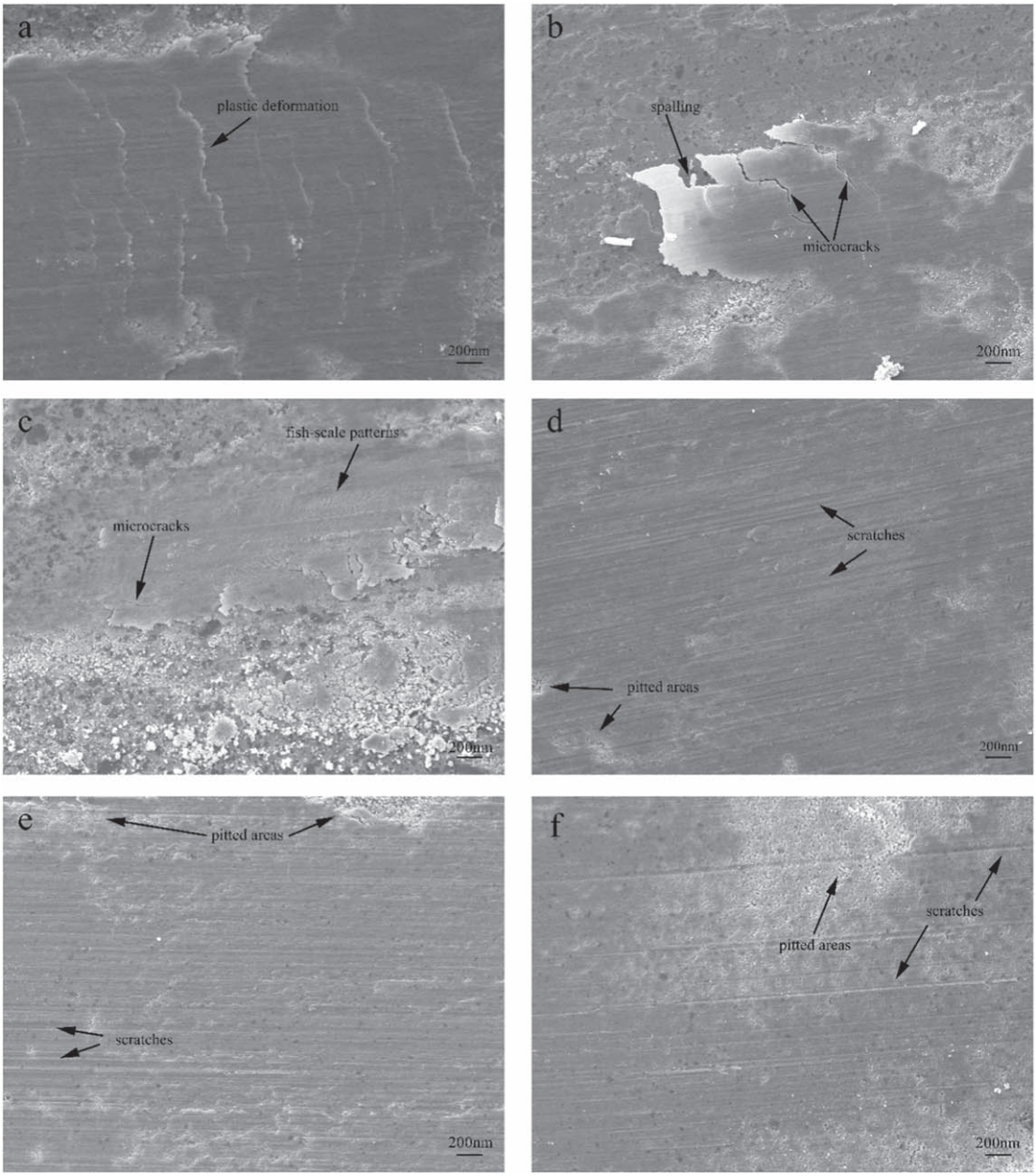


**Figure 13.** The surface morphology after wear of the YSZ ceramics sintered at 1350 °C for 2 h with different contents of $TiO_2$ added: (a) 0 wt%, (b) 1.0 wt%, (c) 3.0 wt%, (d) 5.0 wt%, (e) 7.0 wt%, and (f) 10.0 wt%.

$$\delta = V/(L \times N) \tag{2.2}$$

Where $\delta$ is the volume wear rate, $V$ is Volume of wear ($mm^3$), $L$ is the sliding distance (mm), $N$ is the load (N). The volume wear rate varies, similar to the friction coefficient. This result suggests that the wear resistance increases with the addition of $TiO_2$, but when the content of $TiO_2$ exceeds 5.0 wt%, $TiO_2$ addition harms the wear resistance.

To help understand the wear mechanism of the different samples, the surface morphology of each sample after wear is shown in figure 13.

The observed morphologies indicate that plastic deformation, microcracks, surface spalling and pitted areas occur on the worn surface. Typical plastic deformations appear on the worn surface of the sample with 0 wt% $TiO_2$ added (figure 13(a)). The plastic deformation may attributable to the adhesion and smearing of small wear debris particles [42]. Microcracks and surface spalling were observed on the worn surface of the sample with 1 wt% $TiO_2$ added (figure 13(b)). Fatigue processes caused by repeated abrasion on the top surface and the corresponding plastic deformation of the surface result in microcracking [38], and these are attributable to the coalescence of sub-surface cracks in zones that contain a high density of microwear markings, leading to the

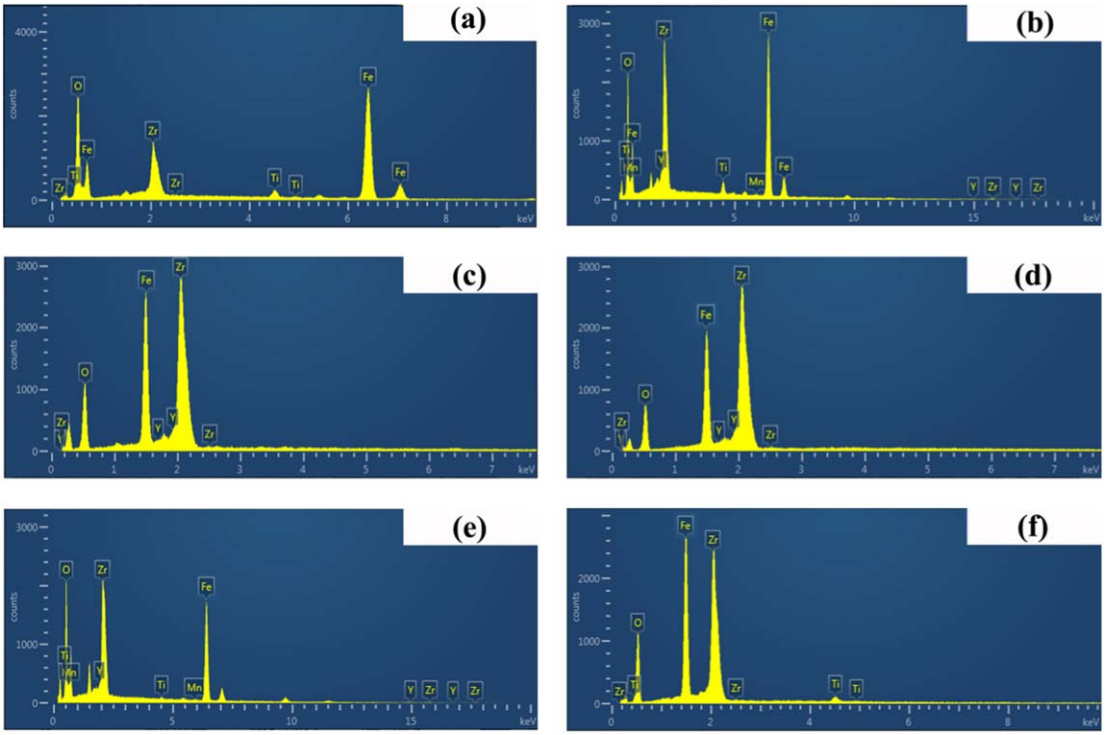


**Figure 14.** The energy spectra of the YSZ ceramics sintered at 1350 °C for 2 h with different amounts of $TiO_2$ added: (a) 0 wt%, (b) 1.0 wt%, (c) 3.0 wt%, (d) 5.0 wt%, (e) 7.0 wt%, and (f) 10.0 wt%.

formation of larger wear particles, or spalling [43–45]. The sample with 3 wt% added $TiO_2$ displays a worn surface (figure 13(c)), where the wear debris is squeezed into layers exhibiting a fish scale pattern, as well as visible microcracks. Similar wear morphology has been observed in prior references [43]. Marked pits and scratches have been observed on the worn surface of samples with $TiO_2$ content in excess of 5 wt% (figures 13(d)–(f)). The coalescence of subsurface cracks causes wear particles to form and pull out, resulting in visible pits on the worn surface [46]. Due to the presence of dislodged wear particles, subsequent sliding moves the microcontacts along, resulting in the observed scratches [47]. Similar wear mechanisms during sliding of zirconia have been reported in previous literatures [44, 48–50].

To identify the element composition of the wear debris, energy spectra have been taken. The energy spectra of the worn surfaces of the YSZ ceramics with different amounts of $TiO_2$ contents are shown in figure 14, with the scan position indicated by the rectangles in figure 15. Mainly Zr, O, and Fe exist on the worn surface, indicating that the debris is mainly composed mainly of scrap iron and $ZrO_2$ particles. This result is consistent with the results reported in the literature [45].

## 4. Conclusions

YSZ ceramics with $TiO_2$ added were prepared by pressureless sintering, and the microstructure, phase evolution, and mechanical properties (micro-hardness, bending strength, and wear resistance) were investigated.

1. $TiO_2$ is a beneficial additive to promote sintering densification in YSZ ceramics. With an increase of $TiO_2$ content from 0 wt% to 10.0 wt%, the relative density of the YSZ ceramics increases from 91.5% to 96.2%.
2. The addition of $TiO_2$ promotes the growth of ceramic grains and the compactness of the YSZ ceramic grain structure. In addition, the addition of $TiO_2$ stabilizes more tetragonal phases to room temperature.
3. With an increase of $TiO_2$ content from 0 wt% to 10.0 wt%, the bending strength of the YSZ ceramics increases from 196.13 MPa to 312.56 MPa. The maximum hardness of the samples is 1792.5 HV, and the minimum volume wear rate is $2.06 \times 10^{-4}$ $mm^3$ $N^{-1} \times m$, when the content of $TiO_2$ is 5.0 wt%. The wear mechanism of $TiO_2$-YSZ ceramics is mainly plastic deformation and microcracking, and the fracturing mechanism within the $TiO_2$-YSZ ceramics primarily involves the intergranular process.

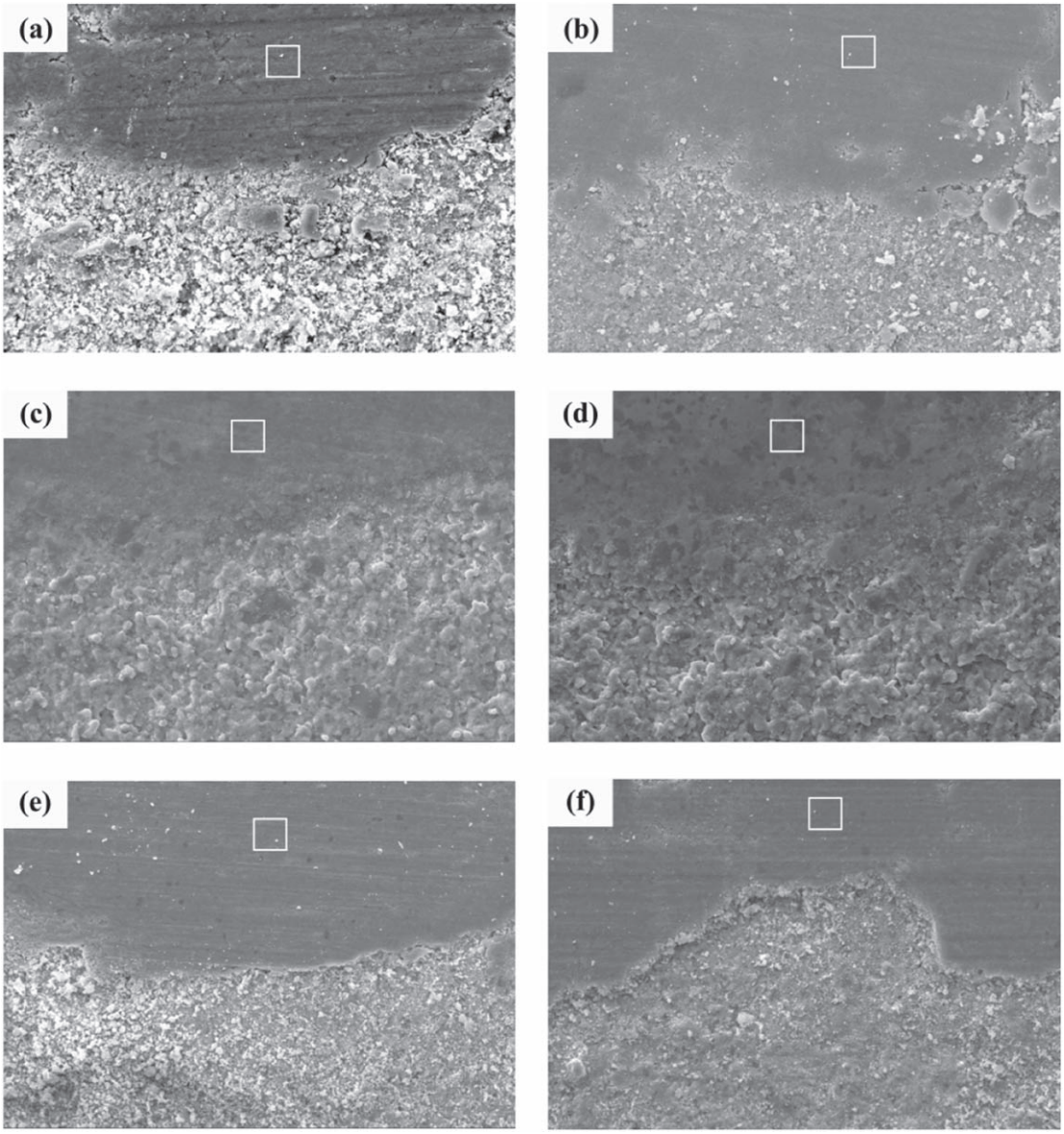


**Figure 15.** The surface morphology after wear of the YSZ ceramics sintered at 1350 °C for 2 h with different contents of $TiO_2$ added: (a) 0 wt%, (b) 1.0 wt%, (c) 3.0 wt%, (d) 5.0 wt%, (e) 7.0 wt%, and (f) 10.0 wt%.

## Acknowledgments

This work was financially supported by the Southwest Petroleum University for the Key Lab of Material of Oil and Gas Field (Grant No. X151516KCL02).

## Conflicts of interest

There are no conflicts to declare.

## ORCID iDs

Jin Zhang https://orcid.org/0000-0002-4643-3800

## References

[1] Kamyshnaya K S and Khabas T A 2016 Developing porous ceramics on the base of zirconia oxide with thin and permeable pores by crystallization of organic additive method *IOP Conf. Ser.: Mater. Sci. Eng.* **156** 012039

[2] Melikhova O, Čížek J, Procházka I, Konstantinova T E and Danilenko I A 2012 Defect Studies of Yttria Stabilized Zirconia with Chromia Additive *Phys. Procedia* **35** 134–9
[3] Xia Y, Mou J, Deng G, Wan S, Tieu K, Zhu H and Xue Q 2020 Sintered $ZrO_2$–$TiO_2$ ceramic composite and its mechanical appraisal *Ceram. Int.* **46** 775–85
[4] Tan P, Wu P, Gao L, Sui Y and Jiang Y 2019 Influence of $Si_3N_4$ content on the physical and mechanical properties of zirconia-toughened alumina (ZTA) ceramic composites *Mater. Res. Express* **6** 065205
[5] Garvie R C, Hannink R H and Pascoe R T 1975 Ceramic steel *Nature* **258** 703–4
[6] Procházka I, Čížek J, Melikhova O, Kuriplach J, Anwand W, Brauer G, Konstantinova T E, Danilenko I A and Yashchishyn I A 2012 Defect Behaviour in Yttria-Stabilised Zirconia Nanomaterials Studied by Positron Annihilation Techniques *Defect. Diffus. Forum* **331** 181–99
[7] Scott H G 1975 Phase relationships in the zirconia-yttria system *J. Mater. Sci.* **10** 1527–35
[8] Park J S, Park C O, Kim H J and Miura N 2005 Low temperature oxygen sensor using YSZ|$\beta-\beta''$ alumina bielectrolyte *Solid State Ionics* **176** 1371–5
[9] Minh N Q 1993 Ceramic Fuel Cells *J. Am. Ceram. Soc.* **76** 563–88
[10] Guo S and Kagawa Y 2007 Isothermal and cycle properties of EB-PVD yttria-partially-stabilized zirconia thermal barrier coatings at 1150 and 1300 °C *Ceram. Int.* **33** 373–8
[11] Pandey A K and Biswas K 2011 Influence of sintering parameters on tribological properties of ceria stabilized zirconia bio-ceramics *Ceram. Int.* **37** 257–64
[12] Matsumoto R L K 1988 Aging Behavior of Ceria-Stabilized Tetragonal Zirconia Polycrystals *J. Am. Ceram. Soc.* **71** C128–9
[13] Miyazaki H 2009 The effect of $TiO_2$ additives on the structural stability and thermal properties of yttria fully-stabilized zirconia *J. Therm. Anal. Calorim.* **98** 343–6
[14] Srdić V V, Winterer M and Hahn H 2010 Sintering behavior of nanocrystalline zirconia doped with alumina prepared by chemical vapor synthesis *J. Am. Ceram. Soc.* **83** 1853–60
[15] Ma D, Chen H, Cheng X, Gao K, Wang L, Zhang L, Wang H, Zhang R and Lu H 2019 Preparation and properties of ZTA ceramics using blast furnace slag as sintering additives *Mater. Res. Express* **6** 065201
[16] Bagley R D, Cutler I B and Johnson D L 1970 Effect of $TiO_2$ on Initial sintering of $Al_2O_3$ *J. Am. Ceram. Soc.* **53** 136–41
[17] Hamano K, Hwang S S, Nakagawa Z E and Ohya Y 1987 Effects of $TiO_2$ on sintering of alumina ceramics *International Journal of High Technology Ceramics* **3** 84
[18] Erkalfa H, Misirli Z and Baykara T 1998 The effect of $TiO_2$ and $MnO_2$ on densification and microstructural development of alumina *Ceram. Int.* **24** 81–90
[19] Mishra R S, Mukherjee A K, Yamazaki K and Shoda K 1996 Effect of $TiO_2$ doping on rapid densification of alumina by plasma activated sintering *J. Mater. Res.* **11** 1144–8
[20] Sathiyakumar M and Gnanam F D 2002 Influence of MnO and $TiO_2$ additives on density microstructure and mechanical properties of $Al_2O_3$ *Ceram. Int.* **28** 195–200
[21] Manshor H, Md Aris S, Azhar A Z A, Abdullah E C and Ahmad Z A 2015 Effects of $TiO_2$ addition on the phase, mechanical properties and microstructure of zirconia-toughened alumina ceramic composite *Ceram. Int.* **41** 3961–7
[22] Khaskhoussi A, Calabrese L, Bouaziz J and Proverbio E 2017 Effect of $TiO_2$ addition on microstructure of zirconia/alumina sintered ceramics *Ceram. Int.* **43** 10392–402
[23] Tsukuma K 1986 Transparent titania-yttria-zirconia ceramics *J. Mater. Sci. Lett.* **5** 1143–4
[24] Hidetoshi M 2010 Influence of $TiO_2$ solid solution on the thermal property and ionic conductivity of partially stabilized zirconia *Int. J. Appl. Ceram. Technol* **5** 490–8
[25] Chen T, Tekeli S, Dillon R P and Mecartney M L 2008 Phase stability microstructural evolution and room temperature mechanical properties of $TiO_2$ doped 8mol% $Y_2O_3$ stabilized $ZrO_2$ (8Y-CSZ) *Ceram. Int.* **34** 365–70
[26] Vander Voort G 1998 Inclusion ratings: past, present, and future *Proceedings of the 1996 Symposium on Bearing Steels: Into the 21st Century (New Orleans, LA, USA, 1996)* (https://www.researchgate.net/publication/286548879_Inclusion_ratings_Past_present_and_future)
[27] Wang C J and Huang C Y 2008 Effect of $TiO_2$ addition on the sintering behavior, hardness and fracture toughness of an ultrafine alumina *Mater. Sci. Eng., A* **492** 306–10
[28] Mchale A E and Roth R S 2010 Low-temperature phase relationships in the system $ZrO_2$–$TiO_2$ *J. Am. Ceram. Soc.* **69** 827–32
[29] Troitzsch U and Ellis D J 2004 High-PT study of solid solutions in the system $ZrO_2$–$TiO_2$: the stability of srilankite *Eur. J. Mineral.* **16** 577–84
[30] Lin C L, Gan D and Shen P 1990 The effects of $TiO_2$ addition on the microstructure and transformation of $ZrO_2$ with 3 and 6 mol% $Y_2O_3$ *Mater. Sci. Eng., A* **129** 147–55
[31] Tekeli S, Chen T, Nagayama H, Sakuma T and Mecartney M L 2007 High-temperature deformation behaviour of $TiO_2$-doped 8 mol% $Y_2O_3$-stabilized $ZrO_2$ (8Y-CSZ) under tension and compression *Ceram. Int.* **33** 869–74
[32] Tsurui K 1996 A unique role of $TiO_2$ on the superplastic flow in tetragonal zirconia polycrystals *Scr. Mater.* **34** 443–7
[33] Capel F, Moure C, Durán P, González-Elipe A R and Caballero A 1999 Structure-properties relationships in $TiO_2$-doped stabilized tetragonal zirconia ceramics *Ceram. Int.* **25** 639–48
[34] Miao X, Sun D, Hoo P W, Liu J, Hu Y and Chen Y 2004 Effect of titania addition on yttria-stabilised tetragonal zirconia ceramics sintered at high temperatures *Ceram. Int.* **30** 1041–7
[35] López-López E, Baudín C, Moreno R, Santacruz I, Leon-Reina L and Aranda M A G 2012 Structural characterization of bulk $ZrTiO_4$ and its potential for thermal shock applications *J. Eur. Ceram. Soc.* **32** 299–306
[36] Evans A G and Wilshaw T R 1976 Quasi-static solid particle damage in brittle solids—I observations analysis and implications *Acta Metallurgica* **24** 939–56
[37] Fischer T E, Anderson M P and Jahanmir S 1989 Influence of Fracture Toughness on the Wear Resistance of Yttria-Doped Zirconia Oxide *J. Am. Ceram. Soc.* **72** 252–7
[38] He Y, Winnubst L, Burggraaf A J, Verweij H, Th Van der Varst P G and With B D 1996 Grain-size dependence of sliding wear in tetragonal zirconia polycrystals *J. Am. Ceram. Soc.* **79** 3090–6
[39] Rice R W 2008 Micromechanics of microstructural aspects of ceramic wear *Ceramic Engineering and Science Proceeding* 6, 940-58
[40] Choi S R and Bansal N P 2004 Mechanical behavior of zirconia/alumina composites *Ceram. Int.* **31** 39–46
[41] Attaf M T 2003 New ceramics related investigation of the indentation energy concept *Mater. Lett.* **57** 4684–93
[42] Van den Berg P H J and With G D 1991 Wear and strength of Mg-PSZ, worn on hardened steel *J. Eur. Ceram. Soc.* **8** 123–33
[43] Lee S W, Hsu S M and Shen M C 1993 Ceramic wear maps: zirconia *J. Am. Ceram. Soc.* **76** 1937–47

[44] Suh M S, Chae Y H and Kim S S 2008 Friction and wear behavior of structural ceramics sliding against zirconia *Wear* **264** 800–6
[45] Bundschuh W and Gahr K-H Z 1991 Influence of porosity on friction and sliding wear of tetragonal zirconia polycrystal *Wear* **151** 175–91
[46] Borrero-Lopez O, Pajares A, Constantino P J and Lawn B R 2015 Mechanics of microwear traces in tooth enamel *Acta Biomater.* **14** 146–53
[47] Alonso J, Rodríguez-Rojas F, Borrero-López O, Ortiz A L and Guiberteau F 2019 Effect of sintering duration on the sliding-wear resistance of 3Y-TZP dental ceramics *Int. J. Appl. Ceram. Technol.* **16** 1954–61
[48] Hvizdoš P, Mestra Á and Anglada M 2010 Effect of heat treatment on wear damage mechanisms in 3Y-TZP ceramics *Wear* **269** 26–30
[49] Yang C C T and Wei W C J 2000 Effects of material properties and testing parameters on wear properties of fine-grain zirconia (TZP) *Wear* **242** 97–104
[50] Stachowiak G W and Stachowiak G B 1993 Environmental effects on wear and friction of toughened zirconia ceramics *Wear* **160** 153–62